

Slag Control Technology to Improve Electrodeposition Coatability of Arc Weld Joints

Hikaru KINASHI*1 · Yue SUN*2 · Kazuya IKAI*1

*1 Welding Process Department, Technical Center, Welding Business

*2 Welding Process Department, Technical Center, Welding Business (currently Finance and Accounting Department)

Abstract

To improve the durability and reliability of arc weld joints of automobile chassis parts, a welding consumable has been developed that can improve the electrodeposition coatability of weld bead by adjusting the deoxidizing elements in the welding wire. In this paper, the lap fillet weld joints were prepared using conventional and developed wire, and the surface and cross-section of weld slag were observed to investigate the relationship between the oxide state and electrodeposition coating properties. It has been confirmed that the composition of the major oxides in the weld slag of the developed wire is multiple Mn-based oxides, rather than Si-Mn composite oxides. In addition, it has been confirmed that the constitutional state of the Mn-based oxides in the welding slag has changed due to the dilution effect of the base steel plate, and that these factors also affected the electrodeposition coatability.

Introduction

Automobile chassis components, including suspension systems, commonly utilize steel materials. These materials must fulfill the concurrent requirements of high strength, rigidity, fatigue resistance, and corrosion resistance. As for corrosion resistance, there is a need for enhanced performance, given exposure to severe corrosion environments like physical damage from road debris during driving, salt-laden air in coastal regions, and de-icing agents in cold climates.

In practice, a certain level of quality is ensured through measures like the partial adoption of galvanized steel sheets and rust prevention treatments¹⁾, including electrodeposition coating for the entire surface of the components.

For joining automobile chassis components, gas shield arc welding is commonly employed. The welding wire used in gas shield arc welding contains deoxidizing elements such as Si and Mn. These elements react with oxygen dissolved in the molten metal and float up to form welding slag on the bead surfaces, resulting in a sound weld joint. On the other hand, since the welding slag is primarily composed of insulating oxides, mainly silicon oxide, the presence of these on the bead surface prevents the formation of coating in the

electrodeposition coating process after welding. In corrosive environments, it is known that areas where electrodeposition coating has not formed can serve as the starting points for rusting. The results of cyclic corrosion testing conducted on test pieces with lap welding joints created using pulse MIG welding after electrodeposition coating are presented in Fig. 1. It is observed that no electrodeposition coating has formed on the residual slag on the weld joint bead, and corrosion has begun from those areas.

To improve the condition of the electrodeposition coating of the weld joint, it is preferable to remove slag as much as possible beforehand. However, manual slag removal is limited due to its high labor intensity leading to a decrease in production efficiency. Additionally, methods such as shot blasting are available for physically removing slag; however, they not only incur increased costs but also present technological challenges, making their application difficult when it comes to complex shapes. Technology has been proposed for controlling slag during welding because it acts as an inhibiting factor for electrodeposition coating. Some approaches involve welding consumables and the welding process. For example, it has been proposed to deliberately add sulfur (S) to agglomerate welding slag or use processes that suppress the generation of welding slag as much as possible, while allowing the generated slag to agglomerate at the bead toe^{2),3)}. Furthermore, a past report indicates that improving the electrodeposition coatability can be achieved by reducing the amounts of Si and Mn in the welding wire⁴⁾. The present authors have adjusted the balance of deoxidizing element additions in the welding wire, thereby altering the morphology

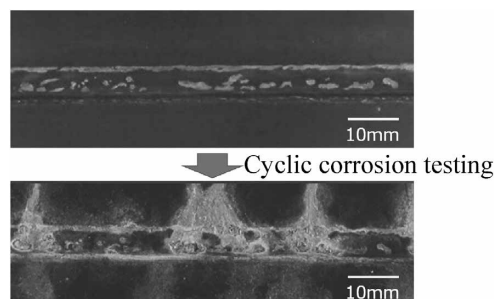


Fig.1 Appearance of weld bead before and after cyclic corrosion testing

and electrical properties of the welding slag. This development allowed for the electrodeposition coating to be formed even in the presence of residual slag in the weld joint. This paper reports the results of comparing the electrodeposition coatability of weld joints using this welding wire with those using the conventional pulse MIG welding wire and also reports on the composition of the welding slag and the internal structure of the oxide in the slag that improves electrodeposition coatability.

1. Test Method

1.1 Test Specimens

Table 1 shows an example of the chemical composition of the welding wire used for the evaluation. As a comparison wire, a pulse MIG welding wire (JIS Z 3312 G 49 A 2 M 16) with a proven track record in welding automobile chassis components was used. The distinctive feature of the developed wire's chemical composition is its extremely low Si content and high content of Mn and Ti. Testing was conducted on a 440 MPa-class hot-rolled steel sheet (SPH440) and a cold-rolled steel sheet (SPCC). **Table 2** presents an example of the chemical compositions of the steel sheets.

1.2 Preparation of weld joint

The welding conditions are presented in **Table 3**. Each steel sheet, with a thickness of 2.3 mm, a width of 50 mm, and a length of 200 mm, were fixed by

a jig as shown in **Fig. 2**. Three sets of lap welding joints were created. The welding process utilized a Digital Power Supply P500L and a welding robot, FD-V8, both manufactured by Daihen Ltd. Pulse MIG welding was conducted under an 80% Ar-20% CO₂ mixed gas. Two sets of the prepared test pieces underwent electrodeposition coating, while the one remaining set was used for the analysis of various slag characteristics.

1.3 Electrodeposition coating

Enlarged photographs were taken of the central part of the bead immediately after welding, and the distribution of slag was noted and entered into comparison for each welding wire and steel sheet. Subsequently, as a pretreatment for electrodeposition coating, the test pieces underwent cleaning, degreasing, surface adjustment and chemical treatment. As a final step, black cationic electrodeposition coating was applied. The target coating thickness was 20 μm.

1.4 Composition and phase analyses of welding slag

From the vicinity of the bead center (the steady part of the bead) of the prepared test pieces, samples for composition analysis were collected through electrical discharge machining. To obtain average composition information about the slag, element analysis was initially conducted using a Scanning Electron Microscope and Energy Dispersive X-ray Spectrometry (SEM-EDS) from the surface side of

Table 1 Chemical composition of welding wires (mass%)

	C	Si	Mn	P	S	Ti
Conventional wire	0.05	0.75	1.25	0.010	0.004	< 0.01
Developed wire (Low Si wire)	0.05	0.10	1.96	0.010	0.006	Add.

Table 2 Chemical composition of steel sheets (mass%)

	C	Si	Mn	P	S	Ti
440MPa steel sheet* (SPH440)	0.12	0.02	0.88	0.014	0.004	< 0.01
Mild steel sheet (SPCC)	0.02	0.01	0.11	0.017	0.002	< 0.01

*Hot rolled sheet.

Table 3 Welding conditions

Robot	FD-V8 (DAIHEN Corporation)
Power supply	Welbee P500L (DAIHEN Corporation)
Welding method	Pulse MAG
Shielding gas	80%Ar-20%CO ₂
Base metal	440 MPa steel sheet (2.3 mmT×50 mmW×200 mmL)
Current-voltage	200 A-24 V
Travel speed	80 cm/min
Travel angle	Perpendicular
Contact-tip to work distance	15 mm

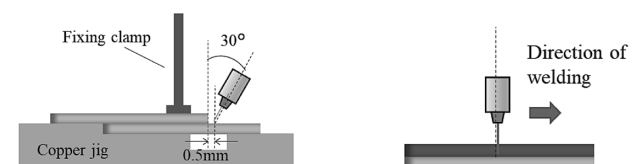


Fig.2 Welding position

the slag. Subsequently, cross-sectional observations of the element distribution in the depth direction of the slag were carried out. The test pieces were embedded in resin and polished. Focusing on the slag location on the upper side of the sheet, where the slag was thickest in the bead cross-section, backscattered electron image observation was performed. For the developed wire, element mapping was conducted using an Electron Probe Micro Analyzer (EPMA). Furthermore, using the multivariate image analysis software, COMPASS, from Thermo Fisher Scientific Inc., phase separation analysis was performed by extracting individual oxide phases with distinctive spectra from the element spectra obtained through EDS⁵⁾.

1.5 Equilibrium state calculation of multi-component oxide

To understand how the composition differences in the welding wire affect the preferential formation of oxide types in the molten slag, equilibrium state calculations of oxides were performed using the thermodynamics equilibrium calculation software FactSage 8.1. In order to simplify the complex relationships among oxides, the calculation was limited to four elements—Si, Mn, Ti, and Fe. The Gibbs energy minimization method was applied to calculate the amount of oxide formed in each temperature range using the thermodynamics data base FToxid. To determine the mass ratio (coefficient) of each oxide in the slag, the coefficients for each oxide were calculated on the basis of the EDS analysis results from the slag surfaces, while ensuring that the sum of the coefficients for all oxides equaled 100.

2. Test results and considerations

2.1 Results of welding and electrodeposition coating

An example of the observed slag behavior on the molten pool during welding is shown in Fig. 3. The welding slag from the conventional wire exhibits a tendency to agglomerate on the molten pool. On the other hand, the welding slag from the developed wire shows suppressed agglomeration on the molten pool and a thin formation on the surface towards the rear of the molten pool. Photos showing the bead appearance after welding and after electrodeposition coating are presented in Fig. 4. The central part of the photo represents the welding bead, with the upper sheet above and the lower sheet below. With the conventional wire, glossy welding slag has been formed on the bead surfaces for both the SPH440

and SPCC steel sheets. In areas where this slag remains, no electrodeposition coating is formed. In contrast, the bead surfaces with the developed wire display a non-glossy dark brown slag that spread uniformly, regardless of the type of steel sheet. Although some areas of the welding slag on the upper sheet side allow no electrodeposition coating to form, the overall area without coating has been significantly reduced compared with the area where conventional wire was used. Focusing on the differences in steel sheets, the SPCC steel sheet exhibits superior electrodeposition coatability for both the conventional and developed wire.

2.2 Observation and composition analysis results for slag surface

The slag formed on the welding beads has been observed as-is on the surfaces using SEM, and composition analysis has been conducted using EDS. Both the conventional wire and the developed wire have been analyzed in the slag near the top sheet side. The positions for the composition analysis of the welding slag using the SPH440 steel sheet are shown in Fig. 5. The square frames indicate the analysis positions, and the circular frames indicate the analysis areas. In the slag from the conventional wire, charge-up traces are observed at the electron beam irradiation positions in the SEM image, suggesting relatively low conductivity. On the other hand, no charge-up traces were observed in the

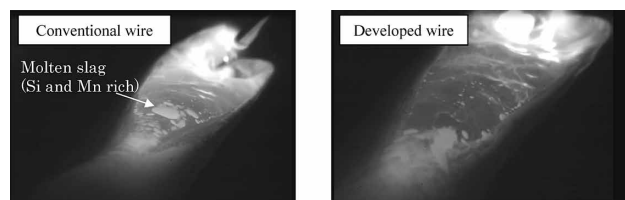


Fig.3 Observation image of molten pool during arc welding (SPH440)

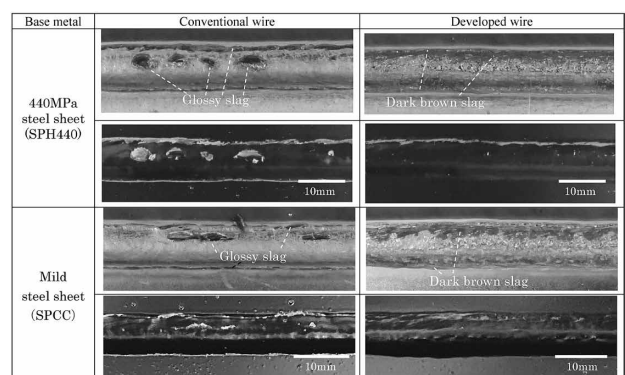


Fig.4 Weld bead appearance (Top: as-welded, Bottom: electrodeposition coated)

brown slag part where the developed wire was used. Next, the EDS analysis results for the welding slag formed using the SPH440 and SPCC steel sheets are shown in Fig. 6. In both the steel sheets, the proportion of Si in the entire slag is higher for the conventional wire. For the developed wire, the proportion of Si in the entire area of slag is smaller, aligning with the intended result that the welding slag is mainly composed of Mn and Ti oxides. Additionally, traces of Fe and minor amounts of Al are detected, which are believed to be inevitably detected in the base metal steel sheet.

2.3 Observation and phase analysis results for slag cross section

2.3.1 Welding slag of conventional wire

Fig. 7 shows the backscattered electron images of the bead cross-sections of the SPH440 steel sheet welded using the conventional wire. The square frames in the figure indicate the locations for slag observation. The thickness of the slag formed in agglomeration near the top sheet side is approximately 200 μm locally. Three morphologies of welding slag are identified: dark areas, bright

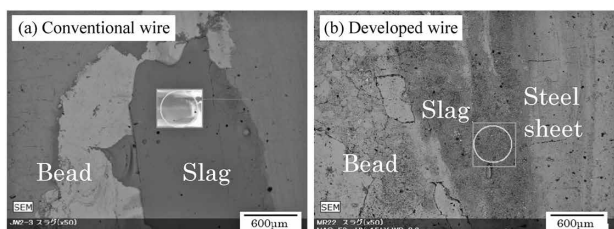


Fig.5 EDS Analysis position (SPH440)

areas, and areas exhibiting distinctive patterns. The results of the oxide phase analysis conducted using COMPASS are presented in Fig. 8. The elements listed in parentheses represent the elements with a higher mass ratio in a phase, in the order from left to right. The slag formed with conventional wire is composed of three main oxide phases: Phase ①, consisting of Mn and Si; Phase ②, consisting of Si and Fe; and Phase ③, consisting of Mn, Si, and Fe. Each of these phases corresponds distinctly to the results of the backscattered electron image observation, clearly existing in separate entities. Consistent with previous findings, it has been confirmed that the glossy slag formed with conventional wire is predominantly composed of oxides, primarily Si and Mn based, throughout the entire region.

2.3.2 Welding slag of developed wire

The developed wire has been used to weld the SPH440 steel sheets. Fig. 9 shows the backscattered electron image of the slag cross-section and

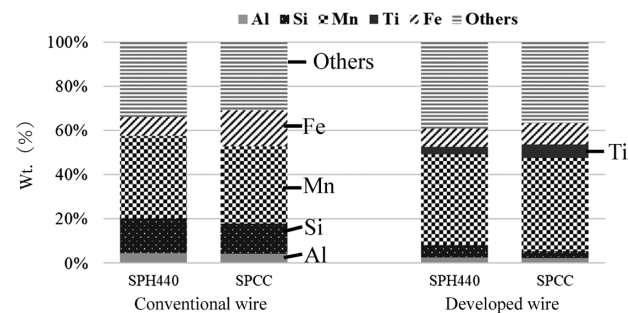


Fig.6 Result of EDS analysis

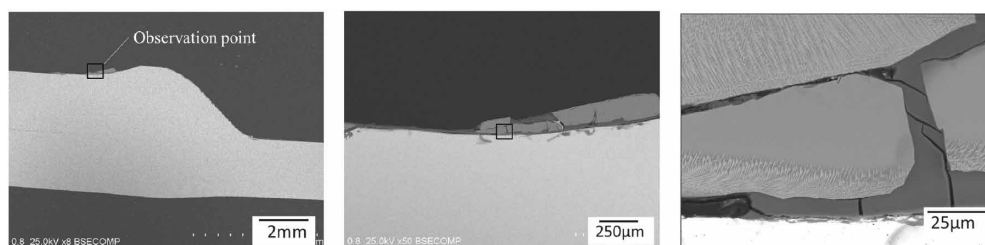


Fig.7 Slag observation point (frame) and backscattered electron (BSE) image (conventional wire, SPH440)

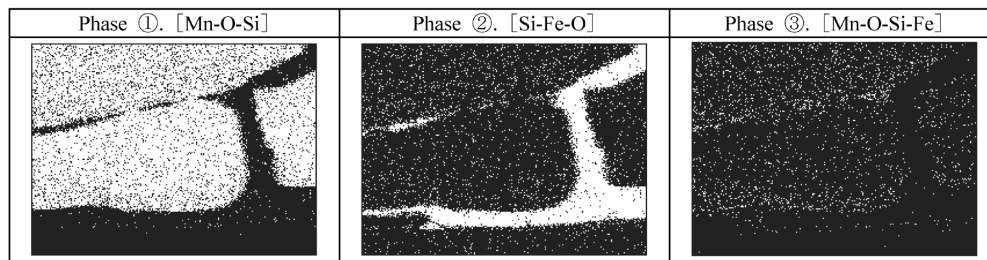


Fig.8 Results of phase analysis [chemical composition] (conventional wire, SPH440)

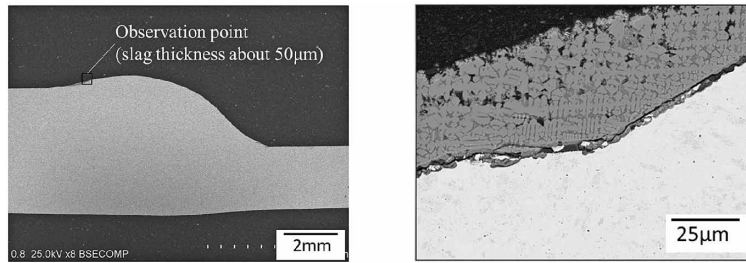


Fig.9 Slag observation point (frame) and BSE image (developed wire, SPH440)

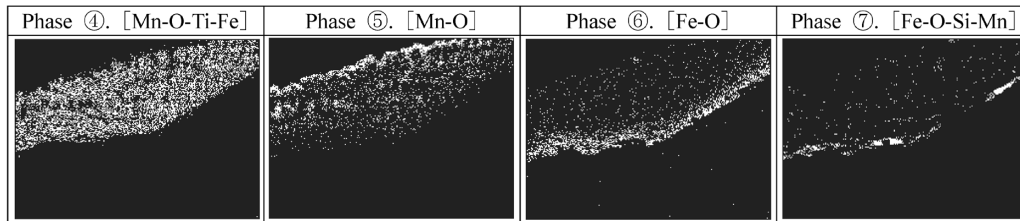


Fig.10 Results of phase analysis [chemical composition] (developed wire, SPH440)

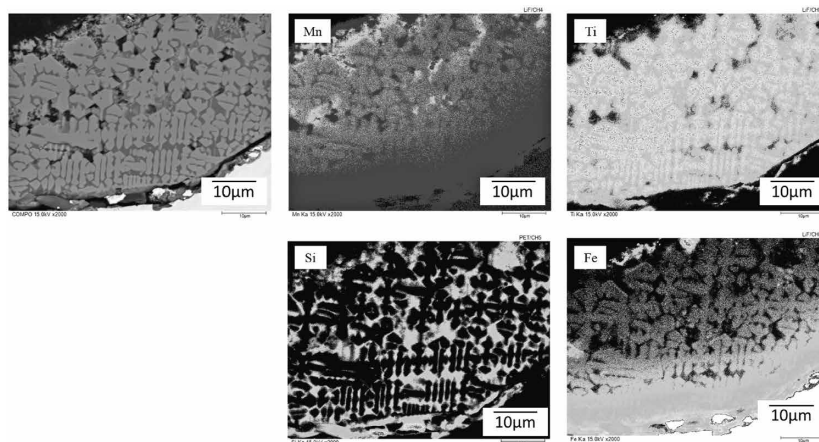


Fig.11 Results of EPMA analysis [chemical composition] (developed wire, SPH440)

enlarged images of the observation points within the square frame. The slag tends to form thickly on the upper side of the sheet, similar to the results of using conventional wire; however, its thickness has been confirmed to be a maximum of about 100 μm , which is thinner than with conventional wire. The morphology of the slag exhibits a dendrite-like structure, a feature not observed in the case of conventional wire. Fig.10 presents the results of oxide phase analysis using COMPASS on the slag formed on the SPH440 steel sheet. The slag is composed of four types of oxide phases: a phase consisting of Mn, Ti, and Fe (Phase ④); Mn oxide phase (Phase ⑤); iron oxide phase (Phase ⑥); and an oxide phase composed of Fe, Si, and Mn (Phase ⑦). Phase ④ is formed throughout the depth direction, Phase ⑤ is formed near the surface of the slag, and Phases ⑥ and ⑦ are distributed on the interface between the slag and the base metal. Unlike the observation results for conventional wire, these

phases are not clearly separated but exist in an overlapping manner. The mapping results of the slag part using EPMA are shown in Fig.11. In the areas where dendrite-like crystalline structures appear bright in the backscattered electron image, mainly Mn, Ti, and Fe are condensed, while darker areas primarily contain condensed Si.

2.3.3 Effect of steel sheet composition on welding slag

The effect of the steel sheet composition on welding slag has been examined using the developed wire. Fig.12 shows the cross-sectional backscattered electron image of the welding slag on the SPCC steel sheet, welded using the developed wire, and an enlarged image of the observation points within the square frame. Similar to the SPH440 steel, there is a tendency for the slag to form thickly on the upper side of the sheet, but its

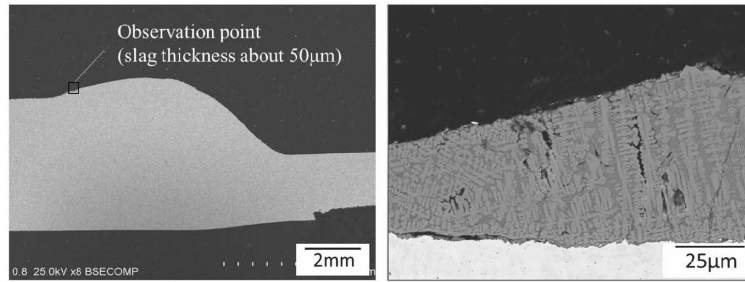


Fig.12 Slag observation point (frame) and BSE image (developed wire, SPCC)

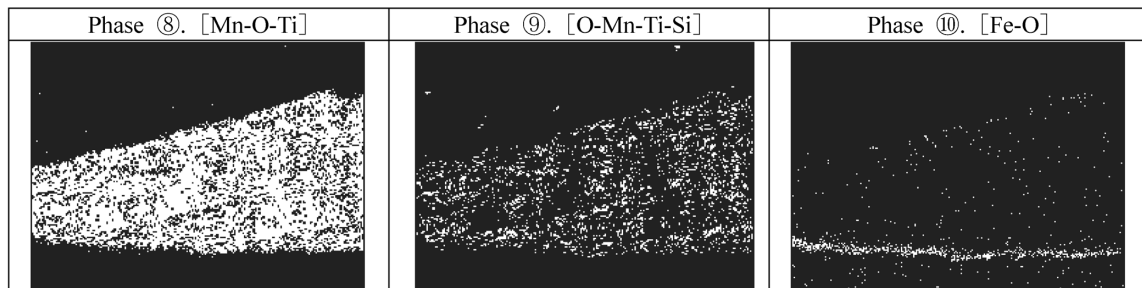


Fig.13 Results of phase analysis [chemical composition] (developed wire, SPCC)

thickness has been confirmed to be a maximum of about 50 μm , and the slag exhibited a dendrite-like morphology on the SPCC steel sheet as well. Fig.13 presents the results of oxide phase analysis using COMPASS for the slag formed on the SPCC steel sheet. The slag is composed of three major phases, with a notably high ratio of oxide phase consisting of Mn and Ti (Phase⑧) and oxide phase consisting of Mn, Ti, and Si (Phase⑨). Additionally, iron oxide phase (Phase ⑩) is observed near the interface with the base metal. In the SPCC steel sheet, as in the SPH440 steel sheet, the main component of the slag is oxide composed of Mn and Ti.

In Fig.10, the surface condensation layer of Mn oxide observed in the SPH440 steel sheet is not observed on the SPCC steel sheet. This suggests that the significantly lower amount of Mn in the SPCC steel sheet, as compared with the SPH440 steel sheet, may be influencing this outcome.

2.3.4 Effect of welding slag thickness on electrodeposition coatability

To assess the effect of slag thickness on the state of electrodeposition coating, observations have been conducted on the slag cross-section after electrodeposition coating. Fig.14 shows the SEM observation results near the slag for the SPH440 steel sheet welded with the developed wire. Electrodeposition coating has been formed up to a slag thickness of about 40-50 μm , but in the areas where the slag is thicker, no electrodeposition coating has been observed. This implies

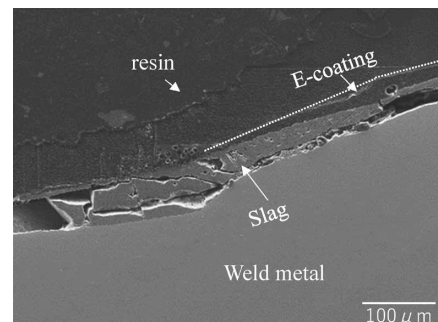


Fig.14 SEM image of weld slag (developed wire, SPH440) after electrodeposition coating)

that reducing slag thickness by suppressing agglomeration may be effective in improving electrodeposition coatability.

2.4 Structure prediction of multi-component oxide by equilibrium state calculation

The results of the equilibrium state oxide calculations for both conventional wire and developed wire are presented in Fig.15. The vertical axis represents the mass fraction of oxides, while the horizontal axis represents the temperature. In the case of the conventional wire, as the temperature decreases from 1800 $^{\circ}\text{C}$ to 1200 $^{\circ}\text{C}$, the molten slag gradually disappears. This means that MnFe_2O_4 begins to form initially, followed by the formation of Si-Mn composite oxides with Olivine structure, such as Mn_2SiO_4 and MnSiO_3 (Rhodonite). Particularly near room temperature, the proportion of Mn_2SiO_4 , a composite oxide of Si and Mn, becomes significant.

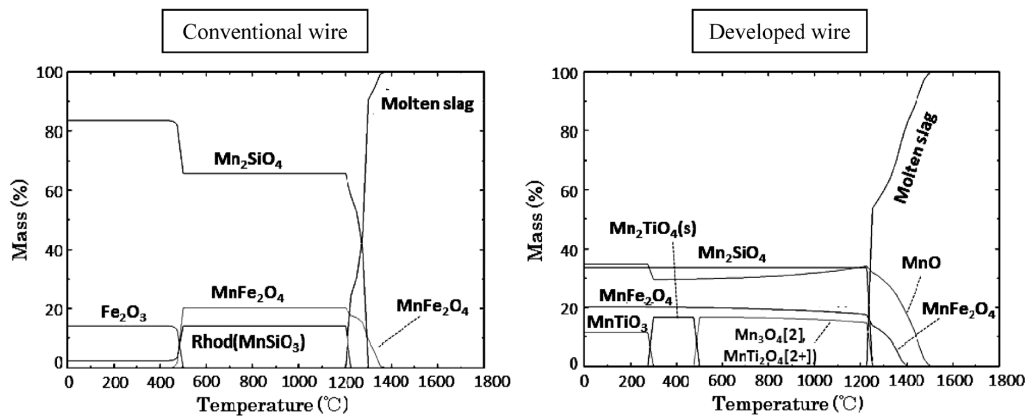


Fig.15 Oxide equilibrium state (effect of temperature on mass percent)

Previous reports have suggested that in the annealing environment of steel sheets with Si and Mn additions, Si and Mn can mutually enhance each other's oxidation reactions, promoting the reduction of iron oxides⁶⁾. It is considered that, even in the deoxidation process during slag formation in arc welding, mutual oxidation reactions (formation of molten slag) are promoted. Moreover, composite oxides of Si and Mn, such as Mn_2SiO_4 and $MnSiO_3$, have lower melting points than composite oxides of Fe and Ti with Mn. As shown in Fig. 3, these Si-Mn composite oxides are likely to reside easily in the molten pool's rearward direction and may persist as thick, large residues during solidification.

Furthermore, the calculation results indicate that Mn_2SiO_4 , an insulating composite oxide of Si and Mn, remains stable on the bead surfaces up to near room temperature after being formed from the molten slag. It is suggested that the preferential formation of these low-conductivity composite oxides during welding, coupled with their local growth through agglomeration, hinders the formation of electrodeposition coating.

On the other hand, in the calculation results for the components of the developed wire, MnO is first formed during the cooling process from the high-temperature side. Subsequently, a composite oxide of Mn and Fe with a spinel structure is formed, followed by the sequential formation of composite oxides with Olivine structure containing Si and Mn, as well as composite oxide of Mn and Ti. Among these, MnO is considered to correspond to the oxide represented by Phase ⑤ in the phase analysis shown in Fig.10. In light of the previous observations of slag cross-sections, it is inferred that in the developed wire, MnO (Monoxide) with higher melting point precipitates ahead of the composite oxide of Mn and Fe during the solidification of the slag formed on the molten pool. Then, the composite oxides of Mn and Si, as well as the composite oxides of

Mn and Ti, begin to form, and these oxides grow in such a way that they overlap, resulting in a dendrite-like solidification morphology. In terms of slag distribution, MnO and the composite oxide of Mn and Fe have a higher solidification initiation temperature and considering the lower ratio of composite oxide of Si and Mn, the agglomeration in the molten pool is less likely to occur, leading to a tendency for the slag to spread thinly. As a result, the conductivity of the slag portion increases, and electrodeposition coatability is inferred to have improved. Considering the conductivity of Mn oxides from the calculation results, MnO is generally known to have lower conductivity at room temperature compared with FeO. Therefore, it is believed that Mn_3O_4 with a spinel structure and composite oxides of Mn and Fe, as well as those of Mn and Ti, contribute to the conductivity. However, since the formed slag consists of multiple oxides overlapping in a complex manner, separating the combined state of individual oxides to identify the specific current paths for the formation of electrodeposition coating is challenging. The mechanism is not yet fully understood, and further investigation and consideration are needed in the future.

Conclusions

By adjusting the balance of deoxidizing element additions in the wire, a welding consumable has been developed that could change the morphology and electrical properties of welding slag, so as to make electrodeposition coating formable even when slag remains in the weld joint. In this report, the composition of slag and the internal structure of oxides within conventional wire and developed wire have been explained in detail, and the factors contributing to improved electrodeposition coatability have been discussed as follows:

- Changing the ratio of Si, Mn, and Ti components in the wire allows control over the ratio of elements constituting the welding slag, resulting in a change in the slag morphology on welding bead surfaces.
- The internal structure of the slag in conventional wire is primarily composed of oxides of Si and Mn throughout, and these oxides are locally thickly formed on bead surfaces.
- In the developed wire, phases of oxides consisting of Mn, Ti, and Fe are formed in the depth direction of the slag, exhibiting a dendrite-like structure. Slag agglomeration behind the molten pool during welding is suppressed, and the slag is formed thinner than for the conventional wire.
- The equilibrium calculation based on the results of slag analysis suggest that Mn oxides with a spinel structure may contribute to the conductivity of the slag in the developed wire.

However, in this investigation, the specific oxides responsible for the conductivity of the slag in the developed wire were not identified. Further research will be conducted to investigate the combined state of oxides constituting the slag and to work towards understanding the mechanism that improves electrodeposition coatability.

References

- 1) Oyabu et al. Transactions ISIJ. 1983, Vol.23, p.994.
- 2) R. Yamazaki et al. R&D Kobe Steel Engineering Reports. 2019, Vol.69, No.1, p.98.
- 3) Umehara et al. Quarterly Journal of the Japan welding society. 2009, Vol.27, No.2, p.163s.
- 4) S. Kodama et al. JSW Technical Review. 2019, Vol.412, p.78.
- 5) M. Wada. Journal of Advanced Science. 2010, Vol.22, No.1&2, p.1.
- 6) S. Maeda et al. Tetsu-to-Hagane. 2018, Vol.104, No.9, p.509.